# Enhanced Deep Learning Approach for Electromagnetic Forward Modeling of Dielectric Target Within the Wide Frequency Band Using Deep Residual Convolutional Neural Network

He Ming Yao<sup>®</sup>, Member, IEEE, Huan Huan Zhang<sup>®</sup>, Senior Member, IEEE, Lijun Jiang<sup>®</sup>, Fellow, IEEE, and Michael Ng<sup>®</sup>, Senior Member, IEEE

Abstract—This letter proposes a novel deep learning (DL)-based fast full-wave broad-band solver to realize electromagnetic forward (EMF) modeling for 2-D dielectric target. This DL-based EMF solver is based on the complex-valued deep residual convolutional neural network (DRCNN), which employs the residual block and deep convolutional operation to improve its generality and performance. While the input of DRCNN combines the incident electromagnetic (EM) field at the arbitrary frequency within the extremely-broad frequency band with the contrasts distribution of the region-of-interest (ROI), the corresponding output is the total EM field illuminated by the input incident EM field. The training data are created based on only the simple synthetic dataset, while the incident EM fields are produced by the sources surrounding ROI. Compared with traditional approaches, EMF modeling has been realized with high accuracy and the greatly reduced computation time. Unlike most of reported DL-based methods, the proposed method can work on the extremely-broad frequency band. Numerical examples based on class-specific 2-D dielectric objects demonstrate the validity of this broad-band EMF solver, which acts as the potential candidate for modeling EMF process in real time.

*Index Terms*—Convolutional neural network, deep learning (DL), deep residual convolutional neural network (DRCNN), electromagnetic forward (EMF) process, real time.

Manuscript received 30 April 2023; revised 6 June 2023; accepted 7 June 2023. Date of publication 4 March 2024; date of current version 4 June 2024. This work was supported in part by the Research Grants Council of Hong Kong under Grant GRF 17207114 and Grant GRF 17210815; in part by the AOARD under Grant FA2386-17-1-0010; in part by NSFC under Grant 61271158, in part by the Hong Kong UGC under Grant AoE/P-04/08; in part by the Hong Kong Research Grant Council under Grant GRF 12300218, Grant 12300519, Grant 17201020, Grant 17300021, Grant C1013-21GF, and Grant C7004-21GF; in part by Joint NSFC and RGC N-HKU769/21; and in part by the Fellowship award from the Research Grants Council of the Hong Kong Special Administrative Region, China, under Grant HKU PDFS2122-7S05. (Corresponding author: Michael Ng.)

He Ming Yao is with the Department of Materials, Imperial College London, London, U.K. (e-mail: yaohmhk@connect.hku.hk).

Huan Huan Zhang is with the School of Electronic Engineering, Xidian University, Xi'an 710071, China (e-mail: hhzhang@xidian.edu.cn).

Lijun Jiang is with the Department of Electronic Engineering, The Chinese University of Hong Kong, Hong Kong (e-mail: ljjiang@ee.cuhk.edu.hk).

Michael Ng is with the Department of Mathematics, Hong Kong Baptist University, Hong Kong (e-mail: michael-ng@hkbu.edu.hk).

Digital Object Identifier 10.1109/LAWP.2024.3372437

## I. INTRODUCTION

ODELING the electromagnetic forward (EMF) process has been referred to an extremely important task for computational electromagnetics (CEM) research [1], [2], [3], [4], [5], [6]. The EMF process have had a wide variety of applications, such as various electromagnetic (EM) inverse problems, antenna design and remote sensing [1], [2], [3]. As a typical CEM-based problem, the key mission of EMF modeling is to solve Maxwell's equations [2], [3], [4], which are discretized and converted into matrix equations. These induced matrix equations usually have the big number of unknowns and will occupy lots of computing resources to solve. Various typical EM computational algorithms, involving finite difference time domain and method of moments (MoM), were proposed for realizing EMF modeling for various practical cases [4], [5], which have usually been transformed into various differential and integral formats [4], [5], [6]. Evidently, traditional techniques for EMF modeling fall short in addressing the demands of real-time application scenarios [4], [5], [6]. Particularly, when faced with intricate situations, EMF-related challenges are characterized by the presence of an enormous number of variables, often reaching into the millions, which unavoidably brings huge computation cost [4], [5], [6]. Therefore, computational efficiency has been a long-standing challenge in EMF modeling [4], [5], [6], [7], [8].

With the development of various high-performance computation platforms, artificial intelligence and machine learning (ML) techniques [9], [10] have been revolutionizing computational science [11], [12], [13], [14]. Meanwhile, the deep learning (DL) technique [15] is being applied into solving different EM problems [16], [17], [18], [19], [20], [21], [22]. In fact, numerous studies have explored the integration of ML strategies to enhance EMF modeling [16], [17], [23], [24], [25], [26], [27]. For instance, Yao et al. [16] explored the innovative integration of artificial neural networks within MoM framework. Plus, by using DL technique, the fast solver to solve Poisson's equations has been introduced for computing the distribution of potential 2-D scenarios by convolutional neural network [17]. In addition, a toy DL-based EMF solver has been proposed, although its application is limited only to several certain EM incident directions and in the specific frequency [26]. Although the application of ML-based models provides the higher efficiency to realize EMF modeling than the conventional methods, most of the reported DL solvers to solve EMF problem can only work on one chosen

 $1536\text{-}1225 \circledcirc 2024 \text{ IEEE. Personal use is permitted, but republication/redistribution requires \text{ IEEE permission.}} \\ \text{See https://www.ieee.org/publications/rights/index.html for more information.}$ 

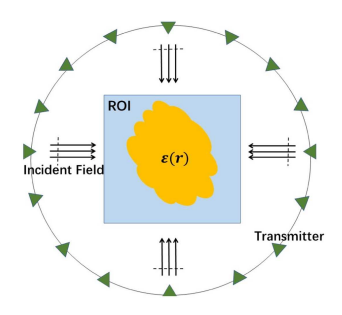


Fig. 1. Modeling setup for ROI: 2-D TMz wave scenario.

frequency [17], [26]. This challenge greatly narrows the range of application for these DL-based EMF solvers.

This work introduces the DL solver for realizing EMF modeling within broad frequency band. This proposed EMF solver has been designed by employing deep residual convolutional neural network (DRCNN). Based on this proposed DRCNN, the total EM field in region-of-interest (ROI) has been successfully computed with low computational cost and high accuracy, which also indicates its potential for being applied to imaging of 3-D metallic targets [27]. Due to its excellent capability, this proposed EMF solver indicates the satisfactory frequency tolerance, so that it can work on the extreme broad frequency band (i.e., 200 MHz–2 GHz).

Thanks to the power of the proposed DRCNN, the merits of the introduced DL method can be encapsulated as follows.

- 1) *Computation efficiency:* This DL-based solver has the potential to address EMF issues in a fraction of the time required by traditional methods, which indicates the possibility of its real-time application;
- 2) Computation accuracy: Due to the application of DL operations, this DL approach can predict total EM field (i.e., realize EMF modeling) with much high accuracy;
- Frequency tolerance: Unlike other reported DL-based methods, the proposed DRCNN can work on the extremely wide frequency band, so that it can deal with various EM incident waves with different frequencies;
- 4) *Model flexibility:* The offline training can integrate more prior information by creating training data, which brings more flexibility to this DL method.

#### II. THEORY AND FORMULATION

# A. Problem Formulation

Fig. 1 depicts the underlying framework for EMF modeling, in which ROI is surrounded by M transmitters. While transmitters could provide EM waves at the arbitrary frequency within a broad frequency band for illuminating EM field of ROI. ROI with target scatterers is divided as uniform  $N \times N$  cells. The transverse magnetic (TM) $_{\rm Z}$  incident field  $E^{\rm in}$  from transmitters at the arbitrary frequency illuminates ROI. Generally, the incident field wave  $E^{\rm in}$  have different frequencies, corresponding to different application scenarios. In the conceptualization of EMF process, the framework is established through the utilization of Lippmann–Schwinger equations [1], [2], [3], where (1) serves as the principal directive [1], [2], [3], [28], characterizing the interplay of fields within the cells located in ROI

$$E^{\text{in}}(\boldsymbol{r}) = E^{t}(\boldsymbol{r}) - k_{0}^{2} \int_{D_{\text{obj}}} G(\boldsymbol{r}, \boldsymbol{r'}) \chi(\boldsymbol{r'}) E^{t}(\boldsymbol{r'}) d\boldsymbol{r'} \quad (1)$$

where  $G(\boldsymbol{r},\boldsymbol{r}')$  is the Green's function within the equation for TMz wave in 2-D space, defined by the expression  $-\frac{j}{4}H_0^{(2)}(k_0|\boldsymbol{r}-\boldsymbol{r}'|)$ , where  $H_0^{(2)}$  denotes the Hankel function of the second kind and zeroth order. The wave number in vacuum is given by  $k_0$ . The coordinates  $\boldsymbol{r}'=(x',y')$  and  $\boldsymbol{r}=(x,y)$  correspond to the locations of the source and observation points, respectively, within ROI. While  $\chi(\boldsymbol{r}')=\varepsilon_r(\boldsymbol{r}')-1$  is the contrast function,  $E^t$  stands for total EM field.

The objective of EMF modeling can be ascertaining the cumulative EM field within ROI as a response to an external EM field. However, directly deriving the comprehensive EM field from (1) is typically an arduous task [1], [2], [3], [4], [5]. Traditional approaches circumvent this by converting (1) into a discretized matrix representation, as indicated by (2) [1], [2], [3], [4], [5]. Based on (2), ROI is divided into uniform cells, of which each has the piece-wise-constant contrast and total EM field. Regrettably, the inherent nonlinearity of (2) presents significant obstacles when tackled with conventional methods [1], [3]. Furthermore, these conventional methods typically demand substantial computational resources due to their inherent complexity [1], [2], [3], [4], [5]. Recently, there are several works attempting to solve (2) by neural-network-based methods [26], [32]. But, these reported DL-based methods can only work on single frequency point rather than the wide frequency band

$$\bar{E}^t = \bar{E}^{\text{in}} + \bar{\bar{G}}_D \cdot \text{diag}\left(\bar{E}^t\right) \cdot \bar{\chi} \tag{2}$$

where the matrix  $\bar{G}_D$  is armed with the size of  $N^2 \times N^2$ .

#### B. DRCNN for Broadband EMF Modeling

For realizing broadband EMF modeling, a new DL approach is introduced by employing DRCNN. The training data created for this DL model relies on the simulation to decline the difficulties of collecting the huge amounts of data based on real experiments. The proposed DRCNN is modified on the basis of the so-called U-Net structure [29], which has been widely applied for image segmentation [30]. The specific internal structure of the proposed DRCNN can be described in Fig. 2. The input of DRCNN consists of EM incident field  $E^{\rm in}$  and contrast  $\chi$ distribution in ROI. Thus, its input has the size as  $N \times N \times 4$  in matrix format, where is  $N \times N$  the number of cells for ROI and the four tubes are the real and imaginary parts of EM incident wave and contrasts of ROI, respectively. Meanwhile, its output is the predicted EM total field  $E^t$  in ROI. Thus, its output has the size as  $N \times N \times 2$ , where  $N \times N$  stands for total number of cells for ROI and the two tubes are the real and imaginary parts of EM total field of ROI.

As presented in Fig. 2, the proposed DRCNN for EMF modeling consists of three paths: encoding, bridging, and decoding. The encoding path encodes the input into information fragments layer by layer, while its corresponding decoding path recovers the final "image" for the expected total EM field. Meanwhile, these two paths are connected by the middle bridging path, where the skip connection are utilized for residual learning between the encoding and decoding paths. The encoding path is equipped with repeated applications of convolution (Conv), batch normalization (BN), and rectified linear unit (ReLU). Here, the encoding path in the proposed DRCNN directly employs convolution rather than max-pooling in conventional U-net to compress "images." Meanwhile, the architecture of the decoding pathway incorporates multiple instances of up-convolution (Upconv), BN, and ReLU activation function. This sequence

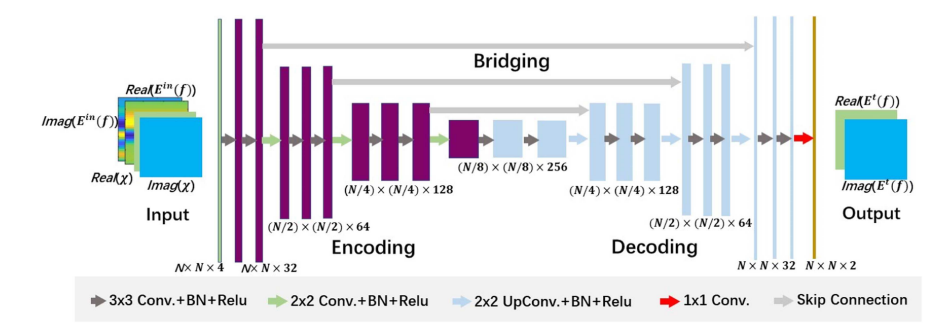


Fig. 2. DRCNN architecture. Conv. is convolution, BN is batch normalization, ReLU is rectified linear unit, Up-conv. is up-convolution, while f represents the randomly selected frequency in the mentioned wideband.

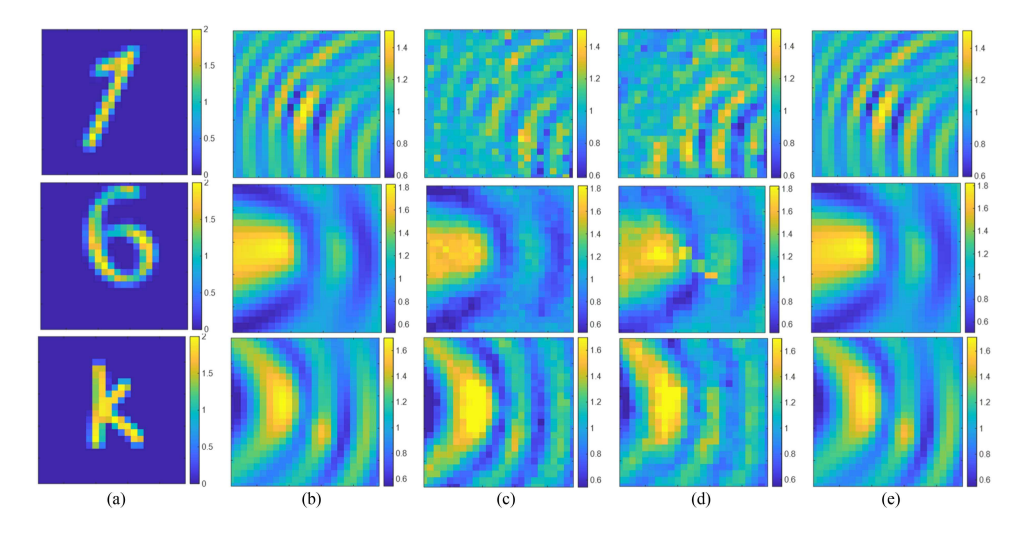


Fig. 3. Comparisons between DRCNN and other methods. (a) Different scatterers with inhomogeneous contrast. (b) MoM result: the computed magnitude of the total EM field  $E^t$  in ROI. (c) MCNN result: the computed magnitude of the total EM field  $E^t$  in ROI. (d) DCED result: the computed magnitude of the total EM field  $E^t$  in ROI. (e) DRCNN result: the computed magnitude of the total EM field  $E^t$  in ROI. The randomly selected frequencies for three samples are: 1.601 GHz for the first sample, 359.6 MHz for the second sample, and 769.5 MHz for the third sample.

culminates with a  $1 \times 1$  convolution layer that finalizes this segment of the network.

A number of important points should be highlighted as follows.

- 1) Input and output of the revised DRCNN: EMF modeling is a typical complex-valued problem. Thus, it is crucial to channel the real and imaginary components of contrast and EM field separately, which enhances the versatility and adaptability of DRCNN, rendering it more suitable for practical application.
- 2) Computational complexity: For this proposed DRCNN, its input has the size as  $N \times N \times 4$ , while its final output, i.e., the total EM field of ROI, has been armed with the size of  $N \times N \times 2$ . As shown in Fig. 3, the basic operations in the proposed DRCNN are Conv, BN, ReLU, and Upconv [30], [35], [36]. Despite the compact size of the filter kernels, it is the convolutional operations that predominantly determine the computational workload. Thus, for the  $N \times N \times 4$  input and the  $N \times N \times 2$  output,  $R \times N \times 4$  filters with the size as  $R_l \times R_l$  in each layer and  $R \times N \times 1$  [30], [39]. Moreover, its memory requirements are largely governed by the dimensions of the filters and the biases. Therefore, the storage of the DRCNN is  $R \times N \times 1$  [30], [39].

#### III. NUMERICAL EXAMPLES

#### A. Numerical Setup and Offline Training

A widely-used dataset, i.e., MNIST, is chosen as the training samples [31], [32], [33], [34], [35], [36]. Based on MNIST, we create training dataset. All selected samples from MNIST have the size as 1 m  $\times$  1 m and are evenly divided as 24  $\times$  24 cells (i.e., N = 24). Meanwhile, transmitters have been randomly located around ROI with the distance to the center of ROI equal to 2 m. Therefore, TM<sub>z</sub> incident waves at the arbitrary frequency (within 200 MHz to 2 GHz) pass from random directions around ROI, which illuminate EM field of ROI from different incident angles. In this letter, the full-wave EM simulations [40] has been utilized to do computation on samples to collect the dataset for training and testing. Selected from the mentioned dataset, the digit-shaped scatterers have the nonhomogeneous contrasts, i.e.,  $\chi$ , ranging from 0 to 2. Fig. 3(a) demonstrates a number of examples of samples. Because of the illumination of random transmitters, 10 000 samples from MNIST are randomly chosen to be scatterers to create training data, while the frequency is randomly selected for each  $E^{\rm in}$  within the range 200 MHz to 2GHz (i.e., 10 000 groups of  $\chi$ ,  $E^{\text{in}}$  and  $E^{t}$  at the arbitrary frequency). The computation of total EM field  $E^t$  is based on traditional MoM [4], [5]. For the purpose of making the appearance of total EM field in ROI more clear, the magnitude of  $E^t$ , named to

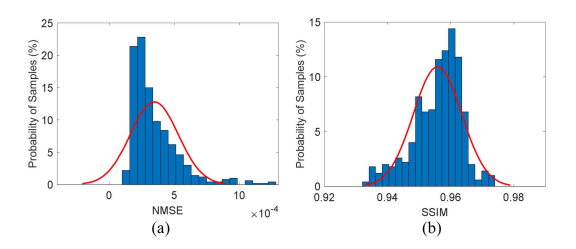


Fig. 4. Statistical histograms of results from DRCNN and fitting of its normal density function and the corresponding MoM results are used as the reference field. (a) NMSE from DRCNN. (b) SSIM from DRCNN.

be "field image," is used to better demonstrate the performance of DRCNN in the next section. To assess the performance of DRCNN, we have selected two metrics: the structural similarity index (SSIM) and the normalized mean-square error (NMSE) [31], [32], [33], [34], [35], [36]. This DRCNN model has been implemented into MATLAB 2021b with the DL Toolbox [37]. Adaptive moment estimation optimizer is utilized to optimize the loss function with the learning rate as 0.001 [38]. During the training, the batch size is set to 250, while the number of epoch is set as 50.

## B. Performance on Different Types of Scatterers

For Section III-B, the performance of DRCNN for EMF modeling has been evaluated based on new unknown samples from MNIST. Several samples from MNIST for testing have been presented in Fig. 3(a). Shown in Fig. 3(b), conventional MoM is utilized to compute the verified total EM field within ROI. Meanwhile, Fig. 3(c) illustrates the corresponding magnitude of  $E^t$  predicted from the DRCNN. In total,1000 new unknown scatterers from MNIST are used to test this trained DRCNN. To indicate the power of our DRCNN, white noise (SNR = 40 dB) has been embedded into  $E^{\rm in}$ . Shown at Fig. 1, ROI with the new unknown sample is illuminated by the incident field  $E^{\rm in}$  at the randomly-selected frequency in the wideband (200 MHz–2 GHz) in unknown incident angles for one single test.

Moreover, to showcase the versatility of this DRCNN, we have curated a novel dataset, termed "Letter," which consists of heterogeneous scatterers, shaped like alphabetic characters, presumed to be distributed randomly within ROI. The attributes for each instance in "Letter" are consistent with those found in MNIST. Furthermore, to display the capability of our DR-CNN, other popular DL-based methods for EMF modeling (i.e., multiply-layer convolutional neural network (MCNN) [14] and deep convolutional encoder—decoder (DCED) structure [26]) have also been adopted as comparison. Shown in Fig. 3, both MCNN and DCED provide bad reconstruction results and suffer from heavy distortion and blurring "texture," which indicates their weak capability of realizing EMF modelling in the wide frequency band.

Fig. 4(a) and (b) indicates an analysis for both NMSE and SSIM based on the predicted magnitude calculated from DR-CNN and the ground-truthed magnitudes of  $E^t$ , where the working frequencies are randomly selected with the mentioned wide frequency band. The NMSE average based on predictions from DRCNN can be only around 0.0004, while the average of SSIM even surprisingly overcomes 0.95. Therefore, the proposed DL solver is able to realize EMF modeling with excellent performance. In addition, while conventional MoM averagely

TABLE I
PERFORMANCE COMPARISON OF DRCNN AND OTHER METHODS

	Computation time on one sample	NMSE (Accuracy)
DRCNN	0.02061s	0.0004
MCNN	0.01174s	0.021
DCED	0.01845s	0.016
MoM	0.7536s	-

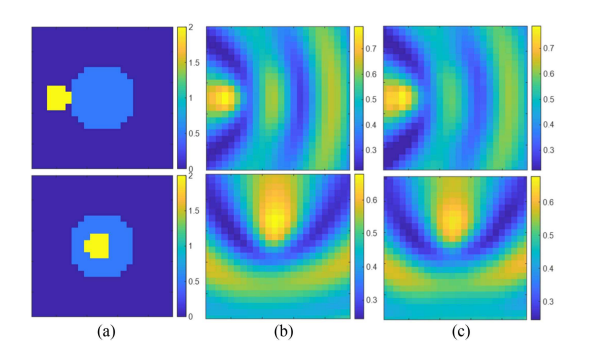


Fig. 5. Comparisons between DRCNN and the conventional method on experimental data. (a) Target scatterers. (b) MoM result: the computed magnitude of the total EM field  $E^t$ . (c) DRCNN result: the computed magnitude of the total EM field  $E^t$ .

uses over 0.75 s to realize EMF modeling for one sample, our DRCNN only uses much less time (about 0.02 s) to complete prediction computation for the same case. Besides, MCNN and DCED utilize about 0.012 and 0.018 s, respectively, to complete computation for one sample. These results indicate the possibility of our DRCNN for its real-time applications at the wide frequency band. The specific comparison can be found in Table I. Moreover, the impact of noise on the trained DRCNN is also be evaluated by adding the noise level of input under different noise levels (SNR). As a result, the NMSE increase from 0.0004 to 0.001 and further to 0.009 for the noise level 40, 30, and 20 dB, respectively, while SSIM decreases from 0.95 to 0.91 and further to 0.63, which indicates the strong capability of this DRCNN. Plus, to remedy degradation caused by the noise, some techniques can be considered, such as data augmentation in training process, the application of dropout and L1/L2 regularization [17].

To further illustrate the capability of our DRCNN, the widely-used experimental data measured at Institute Fresnel are employed [31], [34]. In this experiment (i.e., "FoamDielExt" and "FoamDielInt"), the scatterers consist of two cylinders with the relative permittivity as  $1.45~(\pm 0.15)$  and  $3~(\pm 0.3)$ . We emphasize that only MNIST is still utilized to create new simulation-based training data for the proposed DL method. The retrained DRCNN has demonstrated the excellent performance of predicting the total EM field in Fig. 5.

## IV. CONCLUSION

A DL-based broad-band EMF modeling approach has been introduced by employing DRCNN. Although the training of DRCNN merely relies on the simple synthetic dataset, the proposed DRCNN can realize EMF modeling with excellent accuracy and highly reduced computation cost. Numerical benchmarks based on class-specific 2-D dielectric objects have been utilized to demonstrate the validity of DRCNN. This DL-based EMF modeling approach can meet the requirement of real-time application within the broad frequency band.

#### REFERENCES

- [1] W. Chew, E. Michielssen, and J. M. Song, and J. M. Jin, Eds., *Fast and Efficient Algorithms in Computational Electromagnetics*. Norwood, MA, USA: Artech House, 2001.
- [2] M. Li et al., "Electromagnetic inverse problems [Guest Editorial]," *IEEE Antennas Propag. Mag.*, vol. 59, no. 5, pp. 9–115, Oct. 2017.
- [3] M. Pastorino. Microwave Imaging. Hoboken, NJ, USA: Wiley, 2010.
- [4] A. Bondeson, T. Rylander, and P. Ingelström, Computational Electromagnetics. Berlin, Germany: Springer, 2005.
- [5] R. F. Harrington, Field Computation by Moment Methods. Piscataway, NJ, USA: Wiley-IEEE Press. 1993.
- [6] K. Yee, "Numerical solution of initial boundary value problems involving Maxwell's equations in isotropic media," *IEEE Trans. Antennas Propag.*, vol. AP-14, no. 3, pp. 302–307, May 1966.
- [7] W. Yu and R. Mittra, "A look at some challenging problems in computational electromagnetics," *IEEE Antennas Propag. Mag.*, vol. 46, no. 5, pp. 18–32, Oct. 2004.
- [8] F. Reitich and K. K. Tamma, "State-of-the-art trends and directions in computational electromagnetics," *Comput. Model. Eng. Sci.*, vol. 5, no. 4, pp. 287–294, 2004.
- [9] C. M. Bishop, Pattern Recognition and Machine Learning. Cham, Switzerland: Springer, Aug. 2006.
- [10] E. Alpaydin, Introduction to Machine Learning. Cambridge, MA, USA: MIT Press, 2020.
- [11] H. M. Yao, M. Li, and L. Jiang, "Applying deep learning approach to far-field subwavelength imaging based on near-field resonant metalens at microwave frequencies," *IEEE Access*, vol. 7, pp. 63801–63808, 2019.
- [12] M. Frank, D. Drikakis, and V. Charissis, "Machine learning methods for computational science and engineering," *Computation J. Comput. Eng. Sect. MDPI*, vol. 8, no. 1, 2020, Art. no. 15.
- [13] R. Guo, H. M. Yao, M. Li, M. K. P. Ng, L. Jiang, and A. Abubakar, "Joint inversion of audio-magnetotelluric and seismic travel time data with deep learning constraint," *IEEE Trans. Geosci. Remote Sens.*, vol. 59, no. 9, pp. 7982–7995, Sep. 2021.
- [14] H. M. Yao et al., "Applying convolutional neural networks for the source reconstruction," *Prog. Electromagn. Res. M*, vol. 76, pp. 91–99, 2018.
- [15] Y. LeCun, Y. Bengio, and G. Hinton, "Deep learning," *Nature*, vol. 521, no. 7553, pp. 436–444, 2015.
- [16] H. Yao, L. Jiang, and Y. Qin, "Machine learning based method of moments (ML-MoM)," in Proc. IEEE Int. Symp. Antennas Propag. USNC/URSI Nat. Radio Sci. Meeting, 2017, pp. 973–974.
- [17] T. Shan et al., "Study on a fast solver for Poisson's equation based on deep learning technique," *IEEE Trans. Antennas Propag.*, vol. 68, no. 9, pp. 6725–6733, Sep. 2020, doi: 10.1109/TAP.2020.2985172.
- [18] H. M. Yao, R. Guo, M. Li, L. Jiang, and M. Ng, "Enhanced supervised descent learning technique for electromagnetic inverse scattering problems by the deep convolutional neural networks," *IEEE Trans. Antennas Propag.*, vol. 70, no. 8, pp. 6195–6206, Aug. 2022.
- [19] H. H. Zhang, H. M. Yao, L. Jiang, and M. Ng, "Enhanced two-step deep learning approach for electromagnetic inverse scattering problems: Frequency extrapolation and scatterer reconstruction," *IEEE Trans. Antennas Propag.*, vol. 71, no. 2, pp. 1662–1672, Feb. 2023.
- [20] H. H. Zhang, H. M. Yao, L. Jiang, and M. Ng, "Solving electromagnetic inverse scattering problems in inhomogeneous Media by deep convolutional encoder-decoder structure," *IEEE Trans. Antennas Propag.*, vol. 71, no. 3, pp. 2867–2872, Mar. 2023.
- [21] H. H. Zhang, L. J. Jiang, and H. M. Yao, "Embedding the behavior macromodel into TDIE for transient field-circuit simulations," *IEEE Trans. Antennas Propag.*, vol. 64, no. 7, pp. 3233–3238, Jul. 2016.

- [22] H. H. Zhang, L. J. Jiang, H. M. Yao, and Y. Zhang, "Transient heterogeneous electromagnetic simulation with DGTD and behavioral macromodel," *IEEE Trans. Electromagn. Compat.*, vol. 59, no. 4, pp. 1152–1160, Aug. 2017.
- [23] H. H. Zhang et al., "Deep long-short term memory networks based solving method for the FDTD method: 2D case," *IEEE Microw. Wireless Compon. Lett.*, vol. 33, no. 5, pp. 499–502, May 2023.
- [24] L. Guo, M. Li, S. Xu, F. Yang, and L. Liu, "Electromagnetic modeling using an FDTD-equivalent recurrent convolution neural network: Accurate computing on a deep learning framework," *IEEE Antennas Propag. Mag.*, vol. 65, no. 1, pp. 93–102, Feb. 2023, doi: 10.1109/MAP.2021.3127514.
- [25] H. M. Yao and L. Jiang, "Machine-learning-based PML for the FDTD method," *IEEE Antennas Wireless Propag. Lett.*, vol. 18, no. 1, pp. 192–196, Jan. 2019.
- [26] H. M. Yao, L. Jiang, and M. Ng, "Implementing the fast full wave electromagnetic forward solver using the deep convolutional encoder-decoder architecture," *IEEE Trans. Antennas Propag.*, vol. 71, no. 1, pp. 1152–1157, Jan. 2023, doi 10.1109/TAP.2022.3216920.
- [27] C. Saigre-Tardif et al., "Intelligent meta-imagers: From compressed to learned sensing," Appl. Phys. Rev., vol. 9, no. 1, 2022, Art. no. 011314.
- [28] M. A. Fiddy and R. S. Ritter, Introduction to Imaging from Scattered Fields. Boca Raton, FL, USA: CRC Press, 2014.
- [29] O. Ronneberger, P. Fischer, and T. Brox, "U-net: Convolutional networks for biomedical image segmentation," in *Proc. 18th Int. Conf. Med. Image Comput. Comput. Assist. Intervent.*, 2015, pp. 234–241.
- [30] K. H. Jin et al., "Deep convolutional neural network for inverse problems in imaging," *IEEE Trans. Image Process.*, vol. 26, no. 9, pp. 4509–4522, Sep. 2017.
- [31] R. Guo, X. Song, M. Li, F. Yang, S. Xu, and A. Abubakar, "Supervised descent learning technique for 2D microwave imaging," *IEEE Trans. Antennas Propag.*, vol. 67, no. 5, pp. 3550–3554, May 2019.
- [32] T. Shan, R. Guo, M. Li, F. Yang, S. Xu, and L. Liang, "Application of Multitask learning for 2D modeling of magnetotelluric surveys: TE case," *IEEE Trans. Geosci. Remote Sens.*, vol. 60, 2022, Art. no. 4503709, doi: 10.1109/TGRS.2021.3101119.
- [33] H. H. Zhang, H. M. Yao, L. Jiang, and M. Ng, "Fast full wave electromagnetic forward solver based on deep conditional convolutional autoencoders," *IEEE Antennas Wireless Propag. Lett.*, vol. 22, no. 4, pp. 779–783, Apr. 2023.
- [34] R. Guo et al., "Pixel- and model-based microwave inversion with supervised descent method for dielectric targets," *IEEE Trans. Antennas Propag.*, vol. 68, no. 12, pp. 8114–8126, Dec. 2020.
- [35] H. M. Yao, W. E. I. Sha, and L. Jiang, "Two-step enhanced deep learning approach for electromagnetic inverse scattering problems," *IEEE Antennas Wireless Propag. Lett.*, vol. 18, no. 11, pp. 2254–2258, Nov. 2019.
- [36] H. M. Yao, L. Jiang, and W. E. I. Sha, "Enhanced deep learning approach based on the deep convolutional encoder-decoder architecture for electromagnetic inverse scattering problems," *IEEE Antennas Wireless Propag. Lett.*, vol. 19, no. 7, pp. 1211–1215, Jul. 2020.
- [37] P. Kim, MATLAB Deep Learning. New York, NY, USA: Apress, 2017.
- [38] D. P. Kingma and J. L. Ba, "Adam: A method for stochastic optimization," in *Proc. Int. Conf. Learn. Represent.*, 2015, pp. 1–41.
- [39] J. Cong and B. Xiao, "Minimizing computation in convolutional neural networks," in *Proc. Int. Conf. Artif. Neural Netw.*, 2014, pp. 281–290.
- [40] M. F. Catedra, R. P. Torres, J. Basterrechea, and E. Gago. The CG-FFT Method: Application of Signal Processing Techniques to Electromagnetics. Boston, MA, USA: Artech House, 1995.